

## Giant Straining Process for Production of Ultrafine Structures and High Performance Aluminum

Zenji Horita

Department of Materials Science and Engineering, Faculty of Engineering, Kyushu University, Fukuoka 819-0395, Japan

This presentation summarizes applications of giant straining process (GSP) to aluminum and aluminum alloys. It is shown that the process of grain refinement is significantly affected by the purity of aluminum. High purity aluminum exhibits a unique behavior with straining when it is compared with other pure metals. GSP can be used not only for grain refinement but also for fine dispersion of second phase particles and for consolidation of powders to produce composites with high performance. Recent development of GSP processes is further introduced in this presentation.

**Keywords:** *high-pressure torsion; severe plastic deformation; ultrafine grained; precipitation; composite.*

### 1. Introduction

Giant straining process (GSP) is a promising procedure to refine microstructures and to enhance mechanical and functional properties. In GSP, materials are subjected to severe plastic deformation and thus intense strain is produced in the samples. This processing technology, which is usually called a Severe Plastic Deformation (SPD) process, makes use of the plastic deformation where no change in the cross-sectional dimension of a work piece occurs during straining. Such GSPs include equal-channel angular pressing (ECAP), high-pressure torsion (HPT), accumulative roll bonding (ARB), multidirectional forging (MDF) and many other techniques [1]. Not only grain refinement is feasible to the submicrometer and/or nanometer range but also consolidation of powders is attained with a high packing rate. Because the SPD is a terminology used for large straining of bulk materials [1], GSP is used in the title of this presentation so that powder metallurgy can be incorporated in this acronym.

Among the various GSPs, processing with HPT provides an important advantage over other processing techniques. In the HPT processing, a high pressure in the order of GPa is applied so that not only grain refinement but also fragmentation of second phase particles to the nanosize is feasible. Supersaturation of alloying elements is also achieved and consolidation of metallic powders including amorphous chips and ceramic powders is attained using the HPT processing [2-4].

In this presentation, applications of HPT to aluminum and aluminum alloys are summarized from recent studies. The summary covers the investigation of grain refining process with straining in pure Al, effect of purity level on the grain refinement, dispersion of fine precipitate particles in the small-grained matrix and consolidation of powders to produce nano-composites. This presentation also includes recent development of HPT processing techniques so that HPT can be performed not only using conventional disk samples but also ring and rectangular sheet samples [5,6].

### 2. Application of HPT to Pure Al

Pure Al with a purity level of 99.99% was processed by HPT as schematically illustrated in Fig.1 under a pressure of 1 GPa for 1/8 to 1 revolution using disk samples having 20mm diameter and ring samples having outer diameters of 20, 30 and 40 mm and ring width of 3 mm. Vickers hardness is plotted against the distance from the disk and ring center in Fig.2. For the disk samples, the hardness increases with respect to the distance when the revolution is smaller, and as the revolution becomes larger, the hardness takes a maximum and decreases as the distance is away from the center. For the

ring samples, the values of hardness measured on the ring samples lie on the same levels as the disk samples and the extensions of the disk samples for the corresponding revolutions. When all hardness values are plotted as a function of equivalent strain, they fall on a single curve as shown in Fig.3, taking a maximum at an equivalent strain of  $\sim 2$  and thereafter decreasing to a constant level (steady state). Here, the equivalent strain for HPT is given as

$$\varepsilon = (r\theta/t)/\sqrt{3} \quad (1)$$

where  $r$  is the distance from the center of disk or ring,  $\theta$  is the rotation angle in radian and  $t$  is the thickness of disk or ring.

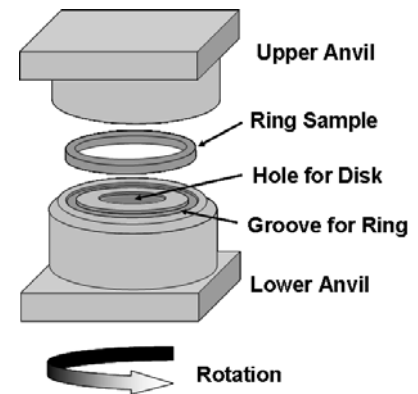


Fig. 1 Schematic illustration of HPT

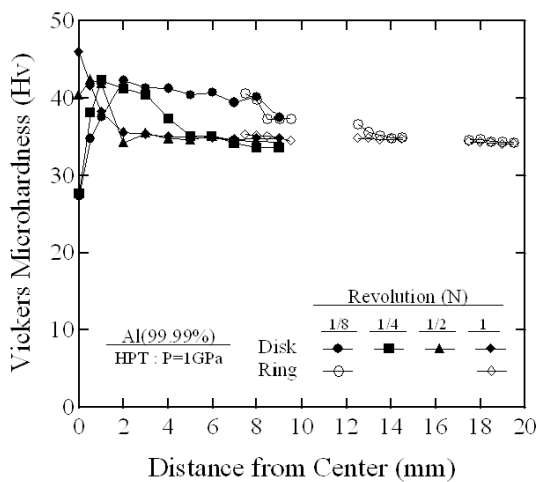


Fig. 2 Hardness variation with distance from center

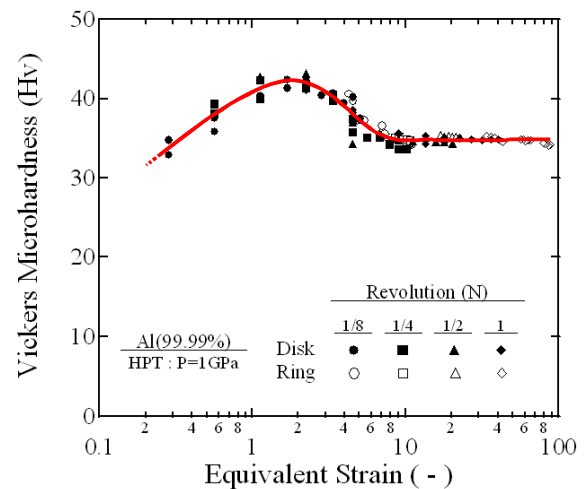


Fig. 3 Hardness variation with equivalent strain.

Figure 4 shows microstructures observed by transmission electron microscopy (TEM) at the equivalent strains corresponding to the hardness maximum, the hardness decrease and the constant level in Fig.3. Many dislocations are present at the hardness maximum but they decrease with straining and few dislocations are visible at the constant level despite the fact that the sample was heavily deformed. Along with this reduction in dislocation density, grain boundaries become smooth and straight with straining, which is a feature resemble to a microstructure after annealing.

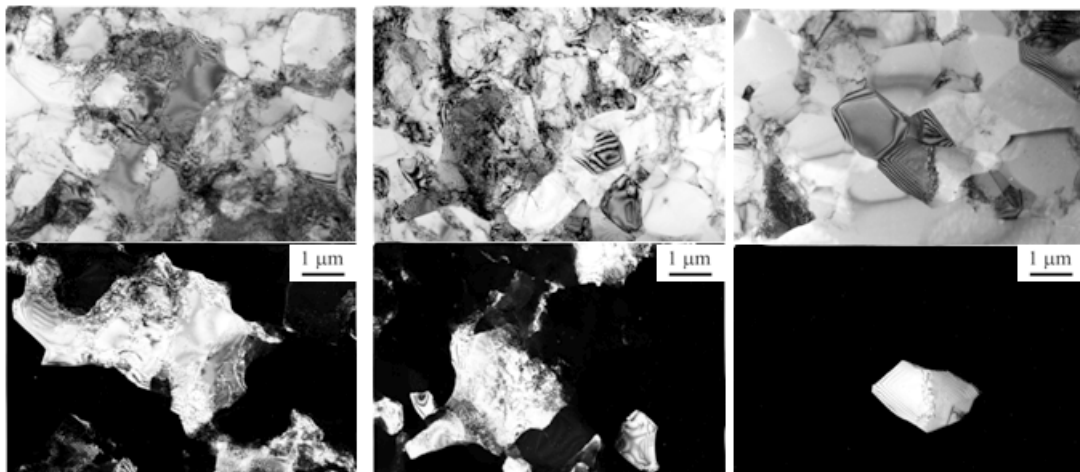


Fig. 4 TEM micrographs at hardness maximum, hardness decrease and steady state.

The hardness variation shown in Fig.3 is sensitive to the purity level as shown in Fig.5. Not only the hardness level is enhanced but also the hardness maximum no longer appears as the purity level is lowered. For the higher purities than 99.99%, the presence of hardness maximum is not prominent in the 99.999% purity and the hardness decreases to the annealed state from the beginning of straining in the 99.9999% purity. These results suggest that dislocation recovery occurs quickly if impurities are too little to pin down the dislocations.

The behavior shown in Fig.3 is in fact unusual when compared with the behavior of other pure metals based on fcc and bcc structures. As demonstrated in a recent paper [7], all hardness values at the steady state fall in a specific range on a universal line as shown in Fig.6 when the normalized hardness  $(HV/G)(T/T_m)$  is plotted as a function of the normalized equivalent strain  $(\epsilon P/G)$  where  $G$  is the shear modulus,  $T$  is the temperature of HPT operation,  $T_m$  is the melting temperature and  $P$  is the applied pressure. For most of the pure metals, the hardness level at the steady state is far higher than that for the pure Al and there is no hardness maximum but the hardness increases and enters directly into the steady state. This unusual behavior appears because pure Al has a high stacking fault energy and thus dislocations are easier to cross slip or climb, which then leads to enhanced annihilation and lowering the hardness level at the steady state. It should be noted that pure Ti exhibits an exceptional behavior. This is partly because a phase transformation occurs during HPT under high pressures although all are not understood yet.

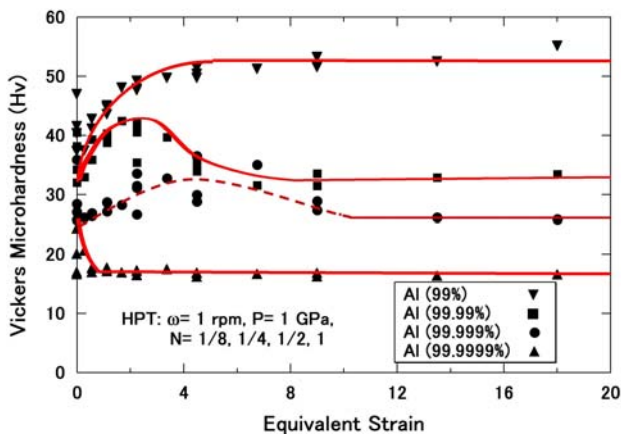


Fig. 5 Hardness variation with equivalent strain for different purities.

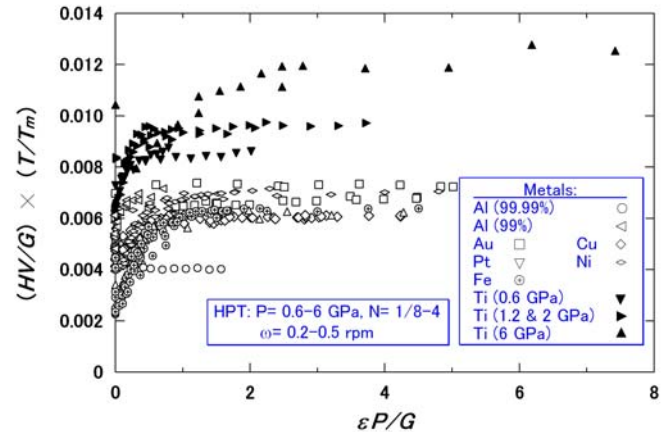


Fig.6 Plots of normalized hardness against normalized equivalent strain for different pure metals [7].

### 3. HPS Processing

The use of a ring sample is promising to scale-up the HPT process. In practice, it was demonstrated that the HPT was successfully attempted with a 100mm ring and 3mm width [8]. It was also shown that the HPT can be operated in a continuous way to produce a sheet form of materials [9]. Alternatively, a sheet sample is processed more directly with the principle as illustrated in Fig.7 [6]. The facility consists of two anvils and one plunger. The plunger has two grooves on the upper and lower surfaces. Each of the upper and lower U-shape anvil has also a groove on the inner bottom surface. The rectangular sheet samples are then placed on the grooves and a load is applied through the anvils. The plunger is then pushed from one side to the other and shear strain is introduced in the sheet under high pressure. This process, designated as high-pressure sliding (HPS) [6], requires no longer rotation of the anvils but sliding between the anvils. Using the HPS, it is possible to process for rectangular sheets and provide a potential to scale-up as in the HPT process for rings. The equivalent strain introduced with this process,  $\epsilon$ , is given by the form as

$$\epsilon = (x/t)/\sqrt{3} \quad (2)$$

where  $x$  is the sliding length and  $t$  is the sample thickness.

The HPS process was attempted on pure Al sheets. The stress-strain curves are shown in Fig.8 after deforming in tension at an initial strain rate of  $1 \times 10^{-3} \text{ s}^{-1}$ . The tensile strength is highest for the sample after 5mm sliding. The strength is reduced to the same level for the longer sliding distances but the total elongation is increased with increasing the sliding distance. The present study demonstrates that the grain refinement is feasible using the process of HPS as other SPD processes. The importance of HPS is that this process is usable under an application of high pressures as in the HPT process but the HPS process is applicable to a form of a rectangular sheet.

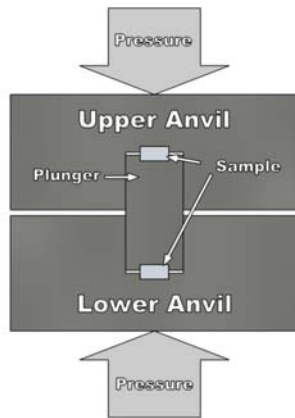


Fig. 7 Schematic illustration of HPS [6].

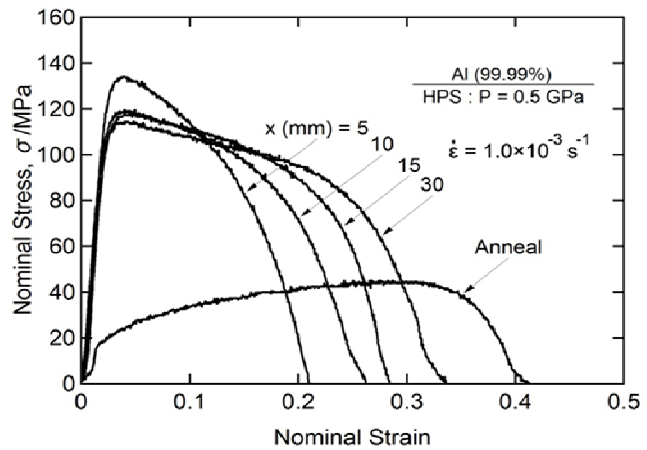


Fig.8 Stress-strain curves of pure Al after different degrees of HPS processing [6].

#### 4. Age Hardening in Ultrafine-Grained Alloys

It is well established that a fine dispersion of precipitate particles during aging enhances the strength of alloys. However, there are limited attempts of aging in ultrafine-grained alloys [10,11]. This is because grain refinement to the submicrometer range is not easy in practice in the alloys with supersaturated conditions using conventional thermomechanical treatment. In addition to this, it is difficult to precipitate very fine particles within the small grains by subsequent aging while keeping the grain size small. The process of severe plastic deformation (SPD) offers a good opportunity for the grain refinement in any type of metallic materials regardless of internal states. Thus, HPT processing was attempted on a 7075 alloy which is known as a typical age-hardenable alloy.

The 7075 alloy was subjected to solution treatment at 753 K for 5 hours and HPT was conducted at room temperature for 3 revolutions under a pressure of 6 GPa. Aging was then undertaken at 373 K for up to the total period of 300 hours. Figure 9 shows changes in Vickers hardness with aging time at several distances from the disk center including the aging behavior without HPT processing. The hardness level is increased as the location becomes closer to the edge of the disk and thus as the strain is more imposed. The hardness increases monotonically with aging and reaches a peak after aging for 30 hours when the imposed strain is small. However, for larger imposed strain as the distance of more than 3 mm from the center, the hardness is initially decreased with aging and then increased to take a peak at 30-hour aging. The highest hardness of 240 HV is achieved for the position 4 mm away from the center.

Figure 10 shows the results of tensile testing conducted at room temperature with the initial strain rate of  $3.3 \times 10^{-3} \text{ s}^{-1}$ . Tensile specimens were cut from the HPT-processed sample at 3 mm away from the disk center with the gauge section of 1mm length, 1mm width and 0.6mm thickness. The tensile strength is significantly increased to 840 MPa by the HPT processing and, by subsequent aging for 30 hours at 373 K, the strength is further enhanced to 930 MPa. The trend for the enhancement of the strength is then consistent with the hardness measurement. By contrast, the ductility is significantly lost by the HPT processing but, nevertheless, there is still 2% for the elongation to failure after the HPT processing and 1 % for the specimen subsequently aged at 373 K for 30 hours.

The microstructure corresponding to the peak aging is shown in Fig.11 with a bright field image on the left, a dark field image at the center and a selected area diffraction pattern on the right. The arrow indicates the diffracted beam for the dark-field image. This microstructural observation reveals that the grain size is reduced to  $\sim 200$  nm or smaller and this ultrafine-grained structure is retained even after aging for 30 hours at 373 K. High resolution electron microscopy confirmed the formation of  $\eta'$  ( $\text{MgZn}_2$ ) and  $\eta$  ( $\text{MgZn}_2$ ) precipitates.

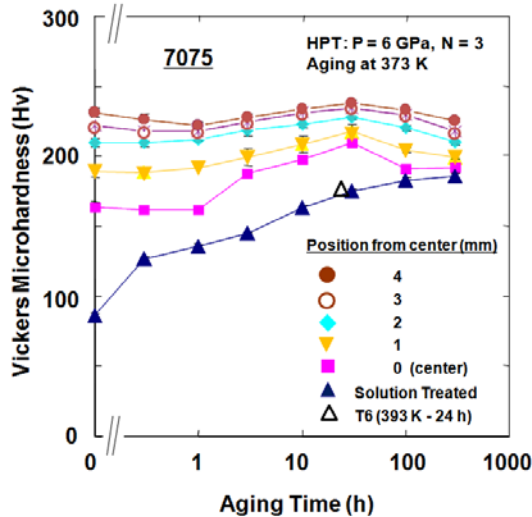


Fig.9 Hardness variation with aging time for 7075 after different processings.

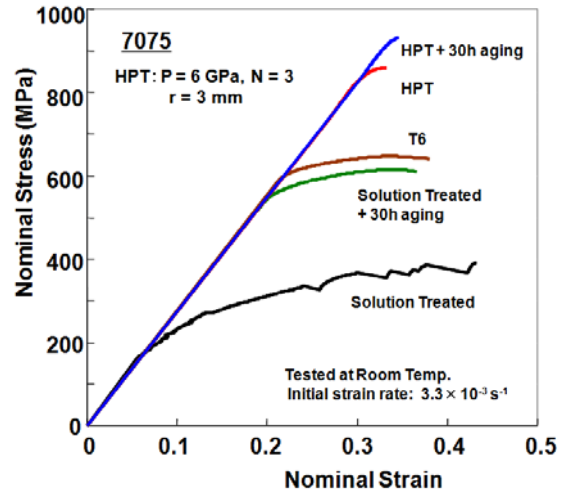


Fig.10 Stress-strain curves of 7075 after different processings.

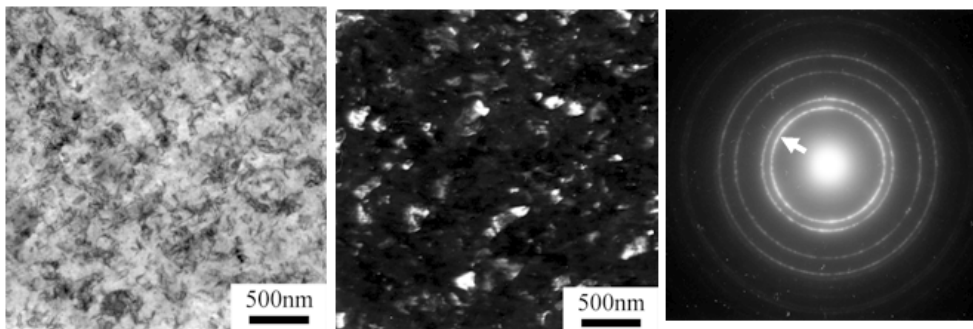


Fig. 11 TEM micrograph at peak aging of HPT-processed 7075.

## 5. Fabrication of Composite without Heating

An Al-based composite containing carbon nanotubes (CNTs) was fabricated using HPT [12]. It is well known that CNTs have high elastic modulus and high tensile strength, typically Young's modulus of 1 TPa and tensile strength of 30 GPa [13]. There have been several attempts to produce Al/CNTs composites but all processes requires heating so that a reaction of CNTs with the Al matrix inevitably occurred to lose the superior properties of CNTs. Al powders were mixed with 5 mass% of the CNTs and subjected to HPT at room temperature with a rotation speed of 1 rpm under a pressure of 2.5 GPa for 30 revolutions.

The Vickers microhardness is plotted in Fig.12 with respect to the distance from the disk center for the samples with and without CNTs including a sample of bulk Al for comparison. The hardness increase is prominent for the sample with CNTs: the value is 36 HV at the disk center but it increases monotonically with the distance to more than twice as 76 HV at 4 mm from the center. There is no essential increase in hardness with the distance for the sample without CNTs. The hardness level is invariably higher in the sample made from powders than the bulk sample. This difference should be due to the presence of alumina layers on the Al powders and dispersed in the Al matrix through the

HPT process. Transmission electron microscopy showed that the grain size of the sample containing CNTs was reduced to  $\sim 100$  nm and this was much smaller than the grain sizes of  $1\sim 2$   $\mu\text{m}$  reported on bulk samples [5]. High resolution electron microscopy revealed that CNTs were present at grain boundaries.

Figure 13 shows the nominal stress plotted against the nominal strain for the HPT samples with and without CNTs. In consistence with the hardness measurement, the sample with CNTs shows higher strength than the sample without CNT. The sample with CNTs also shows a reasonable ductility. It should be noted that, although the total strain to failure is lowered for the sample with CNTs, the uniform strain (corresponding to the strain at the maximum strength in the stress-strain curve) is almost the same as the sample with CNTs. It is important to emphasize that neither heating nor sintering was required with the HPT process so that an *in-situ* consolidation was successfully achieved at ambient temperature with 98% of the theoretical density.

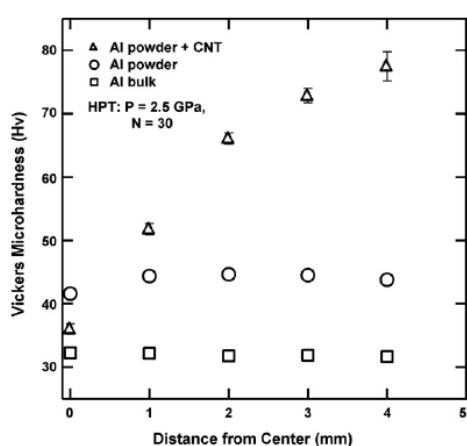


Fig.12 Hardness variation with Al powders with and without CNT after HPT processing [12].

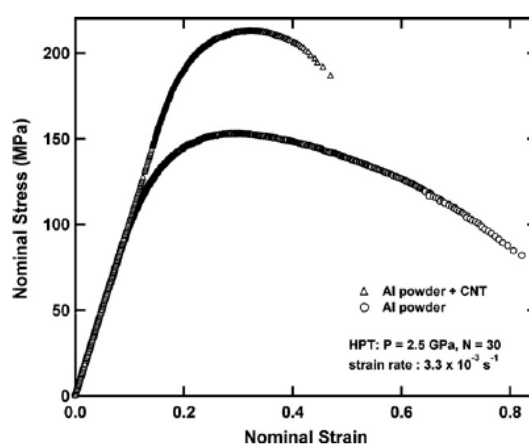


Fig.13 Stress-strain curves of Al powders with and without CNT after HPT processing [12].

## Acknowledgements

This work was supported in part by the Light Metals Educational Foundation of Japan, in part by a Grant-in-Aid for Scientific Research from the MEXT, Japan, in Priority Areas "Giant Straining Process" and in part by Kyushu University Interdisciplinary Programs in Education and Projects in Research Development (P&P).

## References

- [1] R.Z. Valiev, Y. Estrin, Z. Horita, T.G. Langdon, M.J. Zehetbauer, Y.T. Zhu: JOM 58 (4) (2006) 33-39.
- [2] A. P. Zhilyaev and T. G. Langdon: Prog. Mater. Sci. 53 (2008) 893-979.
- [3] K. Edalati, Y. Yokoyama and Z. Horita: Mater. Trans. 51 (2010) 23-26.
- [4] K. Edalati and Z. Horita: Scripta Mater. 63 (2010) 174-177.
- [5] Y. Harai, Y. Ito and Z. Horita: Scripta Mater. 58 (2008) 469-472.
- [6] T. Fujioka and Z. Horita: Mater. Trans. 50 (2009) 930-933.
- [7] K. Edalati and Z. Horita: Mater. Trans. 51 (2010) 1051-1054.
- [8] K. Edalati and Z. Horita: Mater. Trans. 50 (2009) 92-95.
- [9] K. Edalati and Z. Horita: J. Mater. Sci. (2010) in press.
- [10] J.K. Kim, H.G. Jeong, S.I. Hong, Y.S. Kim, W.J. Kim: Scripta Mater 45 (2001) 901-907.
- [11] Z.Horita, K.Ohashi, T.Fujita, K.Kaneko and T.G. Langdon: Adv.Mater. 17 (2005) 1599-1602.
- [12] T. Tokunaga, K. Kaneko and Z. Horita: Mater. Sci. Eng. A 490 (2008) 300-304.
- [13] V. N. Popov: Mater. Sci. Eng. A. 43 (2004) 61-102.